

## Practical Aspects of Proton-Carbon-Carbon-Proton Three-Dimensional Correlation Spectroscopy of $^{13}\text{C}$ -Labeled Proteins

AD BAX, G. MARIUS CLORE, PAUL C. DRISCOLL, ANGELA M. GRONENBORN, MITSUHIKO IKURA, AND LEWIS E. KAY

*Laboratory of Chemical Physics, NIDDK, National Institutes of Health, Bethesda, Maryland 20892*

Received January 4, 1990

The determination of protein solution structures by NMR requires complete assignment of both the backbone and the amino acid side-chain resonances. For larger proteins, such assignments can be difficult to obtain because of extensive resonance overlap in the 2D  $^1\text{H}$ - $^1\text{H}$  correlation spectra. The overlap problem can be substantially reduced by separating homonuclear correlation spectra in a three-dimensional experiment, combining the homonuclear correlation techniques with a heteronuclear multiple-quantum correlation (HMQC) experiment. Such 3D NOESY-HMQC and HOHAHA-HMQC techniques work well for  $^{15}\text{N}$ -labeled proteins (1-3). Very recently, it has been demonstrated that the 3D NOESY-HMQC technique can also be used for  $^{13}\text{C}$ -labeled proteins (4, 5). However, separating homonuclear  $J$ -correlation spectra according to the chemical-shift frequencies of attached  $^{13}\text{C}$  nuclei, as previously used for smaller molecules (6, 7), is inefficient for macromolecules. The main reason for this stems from the severe heteronuclear dipolar line broadening of the protons attached to  $^{13}\text{C}$ , making the  $J_{\text{HH}}$  transfer very inefficient.

Recently, we proposed a new three-dimensional NMR experiment, known as HCCH, in which magnetization is transferred between vicinal protons in a three-step manner (8). In the first step,  $^1\text{H}$  magnetization is transferred to its attached  $^{13}\text{C}$  nucleus via the large and well-resolved  $^1J_{\text{CH}}$  coupling ( $\sim 140$  Hz). In the second step,  $^{13}\text{C}$  magnetization is transferred to its  $^{13}\text{C}$  neighbor(s) via the relatively large  $^1J_{\text{CC}}$  coupling (33-45 Hz). Finally  $^{13}\text{C}$  magnetization is transferred back to  $^1\text{H}$  via the  $^1J_{\text{CH}}$  coupling. To maximize sensitivity, this HCCH experiment requires a high level ( $>90\%$ ) of uniform  $^{13}\text{C}$  labeling.

Since magnetization is transferred through one-bond couplings that to first order are independent of dihedral angles, the transfer efficiency is independent of local geometry, in contrast to conventional homonuclear correlation methods. Because all three individual transfer steps are highly effective, the HCCH experiment transfers a substantial fraction of magnetization from one proton to its vicinal partners, despite the relatively large  $^1\text{H}$  linewidth.

Although spectra previously obtained with the HCCH method show many of the desired correlations, they were plagued by relatively high levels of  $t_1$  noise and spectral artifacts (8). In the present Communication we address the sources of these undesirable features and demonstrate improvements that greatly reduce their intensity.

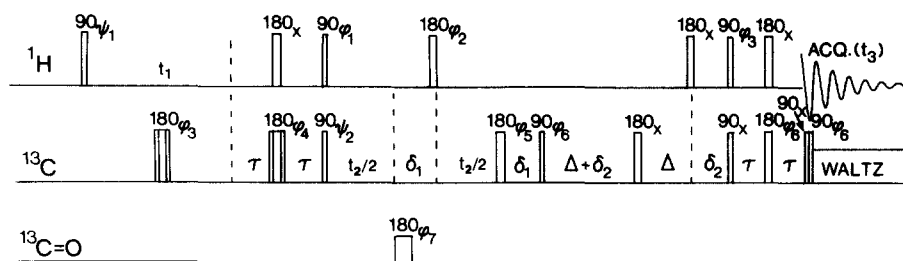


FIG. 1. Pulse sequence of the HCCH 3D experiment. For adequate suppression of artifacts, the sequence requires a 16-step phase cycle:  $\phi_1 = y, -y$ ;  $\phi_2 = 4(x), 4(y), 4(-x), 4(-y)$ ;  $\phi_3 = 8(x), 8(-x)$ ;  $\phi_4 = 2(x), 2(-x)$ ;  $\phi_5 = 2(x), 2(y), 2(-x), 2(-y)$ ;  $\phi_6 = 4(x), 4(-x)$ ;  $\phi_7 = 8(x), 8(y)$ ; Acq. =  $2(x, -x, -x, x), 2(-x, x, x, -x)$ . The  $^{13}\text{C}$  carrier is positioned in the center of the aliphatic region and the  $180^\circ_{\phi_7}$  carbonyl pulse is generated by means of a DANTE sequence. The  $180^\circ_{\phi_3}$  and  $180^\circ_{\phi_4}$  pulses are of the composite type ( $90^\circ_x 180^\circ_y 90^\circ_x$ ). Quadrature in the  $F_1$  and  $F_2$  dimensions is obtained with the TPPI-States method (19), using  $\psi_1 = 16(x), 16(y)$ ;  $\psi_2 = 32(x), 32(y)$ . Each time  $t_1$  is incremented, the receiver reference phase and  $\psi_1$  are also incremented by  $180^\circ$ . Each time  $t_2$  is incremented the receiver phase and  $\psi_2$  are also incremented by  $180^\circ$ . Data obtained for  $\psi_1 = x, y$  and  $\psi_2 = x, y$  are stored separately and processed as complex data.

Figure 1 illustrates the improved HCCH pulse sequence. For the simple case of two coupled carbons,  $C_A$  and  $C_B$  with attached protons  $H_A$  and  $H_B$ , magnetization is transferred from  $H_A$  to  $H_B$  as follows. At the end of the  $^1\text{H}$  evolution period,  $t_1$ , proton magnetization ( $H_A$ ) is transferred to  $^{13}\text{C}$  ( $C_A$ ) in an INEPT-like manner (9, 10). The  $C_A$  transverse magnetization which is antiphase with respect to the polarization of  $H_A$  becomes in-phase during the two delays,  $\delta_1$ , and proton decoupling during the  $t_2$  evolution period is accomplished by the  $180^\circ$   $^1\text{H}$  pulse applied at the center of  $t_2$ . During  $t_2$  (as well as the delays  $\delta_1$ ),  $C_A$  magnetization becomes antiphase with respect to its  $^{13}\text{C}$  coupling partner,  $C_B$ , at a rate that is determined by  $^1J_{CC}$ . The  $90^\circ_{\phi_6}$  pulse subsequently transfers this antiphase  $C_A$  magnetization into antiphase  $C_B$  magnetization in a COSY-type manner. During the following interval,  $2\Delta + 2\delta_2$ , the antiphase  $C_B$  magnetization becomes in-phase with respect to  $C_A$ , and the  $180^\circ$   $^1\text{H}$  pulse (applied at time  $\delta_2$  before the final set of simultaneous  $90^\circ$  pulses) ensures that the refocused  $C_B$  magnetization is antiphase with respect to its attached proton,  $H_B$ . The final sets of  $90^\circ$  and  $180^\circ$  pulses then constitute a reverse refocused INEPT, transferring  $C_B$  magnetization to  $H_B$ .

During repeated use of our original pulse scheme (8), we found two separate problems that cause artifacts and noise-like features in the 3D spectra. It is well known that artifacts generally result from undesired coherence transfer pathways and, as will be discussed later, can be largely removed by extensive phase cycling. The noise-like features were found to originate from modulation sidebands of the composite pulse decoupling cycle used. As pointed out previously (11), these modulation sidebands average to zero if the decoupling is executed in an asynchronous manner and many transients are coadded. Because of the large number of  $t_1$  and  $t_2$  increments required for a 3D experiment, the number of transients per pair of ( $t_1, t_2$ ) values is limited in practice to about 16 because of measuring time constraints. Consequently, averaging of the modulation sidebands is incomplete. The approach we have taken minimizes the amount of composite pulse decoupling in the sequence of Fig. 1, by using  $180^\circ$  pulses at the midpoints of the  $t_1$  and  $t_2$  intervals to remove the net effect of the unde-

sired couplings. However, during the detection period,  $t_3$ , composite pulse decoupling is essential. As will be described in more detail elsewhere, the intensity of modulation sidebands originating from incompletely refocused  $^1\text{H}$  magnetization ( $I_y S_z$  type terms) can be reduced by inserting a  $90_x - 90_{\pm x}$   $^{13}\text{C}$  pulse pair prior to the start of the decoupling, as indicated in Fig. 1. This pulse pair has the effect of inverting  $S_z$  on alternate scans, canceling signals originating from  $I_y S_z$ .

In order to maximize magnetization transfer between the  $C\alpha$  and  $C\beta$  carbons, it is important to remove the effects of  $C\alpha$ -carbonyl coupling during the delays  $t_2 + 2\delta_1$  and  $2\Delta + 2\delta_2$ . For the delay  $2\Delta + 2\delta_2$ , this is accomplished by ensuring that the  $180_x$  pulse causes minimal excitation of the carbonyls. Since the carbonyl resonances are centered at about 177 ppm, whereas the carrier is positioned in the center of the aliphatic region, at 43 ppm, the power and duration of the  $180_x$  pulse must be adjusted such that this pulse has a null in its excitation profile at the carbonyl frequency. During the  $t_2$  period, decoupling is achieved by a  $180^\circ$  pulse applied to the carbonyls. This pulse should be applied in such a way that aliphatic resonances are only minimally affected. Ideally, a shaped selective inversion pulse is used for this purpose. Due to hardware limitations, however, we were forced to use a less ideal but still adequate solution, applying a rectangular carbonyl inversion pulse with low RF power ( $180^\circ$  pulse width  $\sim 400 \mu\text{s}$ ). This carbonyl inversion pulse can be made phase coherent with the other  $^{13}\text{C}$  pulses (avoiding randomness of any spurious excitation of aliphatic resonances) by generating it as a DANTE-type pulse (12, 13). Thus, the carbonyl inversion pulse was applied as eight repetitions of the cycle ( $4_0^\circ$ ,  $4_{-300}^\circ$ ,  $4_{-240}^\circ$ ,  $4_{180}^\circ$ ,  $4_{120}^\circ$ ,  $4_{60}^\circ$ ), where the RF power level is adjusted such that the duration of an individual cycle equals  $1/\delta$ , where  $\delta$  is the offset of the carbonyl resonances from the RF carrier. Long-range couplings between carbonyls and protons are small relative to the  $^1\text{H}$  linewidth, and carbonyl decoupling during the  $t_1$  and  $t_3$  periods is therefore not necessary.

The large variety of relatively weak artifacts found in 3D spectra recorded with our original pulse sequence (8) prompted us to reconsider the phase-cycling scheme used, in order to ensure that only the desired coherence transfer pathway (14) would give rise to magnetization detected during  $t_3$ . In designing a good phase-cycling scheme, a difficult constraint is imposed by the fact that available measuring time limits the number of scans per ( $t_1$ ,  $t_2$ ) pair to at most 16, thus restricting the number of phase-cycling steps.

A single undesired coherence transfer pathway can usually be eliminated by a simple two-step phase cycle. For example, phase inversion of all preparation period pulses in a 2D experiment suppresses axial peaks. If a second source of artifacts must be suppressed additional phase cycling is required. For example, in the case of a NOESY experiment single-quantum coherent transfer can be suppressed by phase alternation of the last pulse. If both types of phase cycling were executed simultaneously (resulting in a two-step cycle), single-quantum coherent transfer of axial signals would not be suppressed in the final spectrum. For this reason, phase-cycling steps are usually executed in an independent manner. For the case of the NOESY experiment, combination of two 2-step phase cycles results in a  $2 \times 2 = 4$ -step phase cycle.

Because of the large number of possible spurious transfer pathways combined with the limited number of available scans per  $(t_1, t_2)$  pair in our present 3D experiment, we were forced to consolidate several of the phase-cycling steps. Two phase cycles may, in general, be executed simultaneously if their purpose is to eliminate two unrelated sources of artifacts. In such a case, if the first phase cycle completely cancels undesired magnetization that would result in an artifact with fractional intensity,  $a$ , and the second phase cycle cancels a second type of artifact of fractional intensity,  $b$ , executing the two phase cycles simultaneously will leave residual artifacts with very low fractional intensity,  $a \times b$ , in the final spectrum.

Using this type of reasoning, supplemented by the experimental results of several dozen trial phase cycles, we developed the 16-step phase cycle given in the legend to Fig. 1, which affords near-optimal suppression of artifacts. In addition, the first two  $180^\circ$   $^{13}\text{C}$  pulses were of the composite type ( $90_x^\circ 180_y^\circ 90_x^\circ$ ) to compensate for offset and RF inhomogeneity effects (15).

The effectiveness of the pulse sequence of Fig. 1 is demonstrated for a 1.8 mM sample of the protein interleukin- $1\beta$  (156 residues, 17 kDa), dissolved in  $\text{D}_2\text{O}$ ,  $p^2\text{H}$  5.2,  $35^\circ\text{C}$ . Spectra were recorded on a Bruker AM-600 spectrometer that had been modified to eliminate overhead time at the end of every  $t_1$  and  $t_2$  increment. The  $^1\text{H}$  carrier was positioned at 3.0 ppm, and the  $^{13}\text{C}$  carrier at 43 ppm. All proton pulses were applied with a 16 kHz RF field.  $^{13}\text{C}$  pulses were applied using a 10 kHz RF field ( $\sim 30$  W RF power), and the DANTE-type carbonyl inversion pulse was applied with a weak 1.3 kHz RF field. For  $^{13}\text{C}$  decoupling during data acquisition, the  $^{13}\text{C}$  power was reduced to 3 W. Acquisition times were 28, 10, and 47 ms in the  $t_1$ ,  $t_2$ , and  $t_3$  dimension, respectively. The size of the acquired 3D matrix was (128 complex)  $\times$  (32 complex)  $\times$  (512 real). Using a delay time of 0.9 s between scans, the total measuring time was 70 h. 3D data were processed with a combination of commercial software (NMRI, Syracuse, New York) and home-written programs for Fourier transformation in the third dimension (13). In all three dimensions,  $50^\circ$ -phase-shifted sine-bell filtering and zero filling were used. For convenience, adjustment of delay durations was used to ensure that zero phase correction was required in both the  $F_1$  and the  $F_2$  dimensions of the final 3D spectrum. Thus, by adding the duration of the composite  $180^\circ$   $^{13}\text{C}$  pulse (100  $\mu\text{s}$ ) to the  $\tau$  delay between the  $180_x^\circ$  and  $90_{\phi_1}^\circ$   $^1\text{H}$  pulses, the required phase correction in the  $F_1$  dimension becomes zero, independent of the  $^1\text{H}$  pulse width. In the  $t_2$  dimension, the  $180_{\phi_2}^\circ$   $^1\text{H}$  pulse is applied at the end of the first  $\delta_1$  interval, eliminating the need for phase correction in the  $F_2$  dimension.

In the  $t_2$  dimension, magnetization transfer between  $J$ -coupled carbons has a  $\sin \pi J_A(t_2 + 2\delta_1) \cos^n \pi J_P(t_2 + 2\delta_1)$  dependence, where  $J_A$  and  $J_P$  are the active and passive carbon-carbon coupling constants,  $J_{CC}$ , and  $n$  is the number of passive carbons. The sum of  $2\delta_1$  plus the  $t_2$  acquisition time is set to about  $1/(2J_{CC})$  and, hence, the  $t_2$  time-domain signal that contributes to the  $^1\text{H}$ - $^1\text{H}$  cross-peak intensity has an envelope shape similar to a sine bell, shifted by  $2\delta_1$ . Thus, the lineshape of a  $^1\text{H}$ - $^1\text{H}$  cross peak in the  $F_2$  dimension is not Lorentzian, and in the absence of digital filtering looks similar to that of a singlet for which resolution enhancement with a shifted sine bell is used. The  $t_2$  time-domain signal of the diagonal ( $F_1 = F_3$ ) resonances has a  $\cos \pi J_A(t_2 + 2\delta_1) \cos^n \pi J_P(t_2 + 2\delta_1)$  dependence, corresponding to a rapidly de-

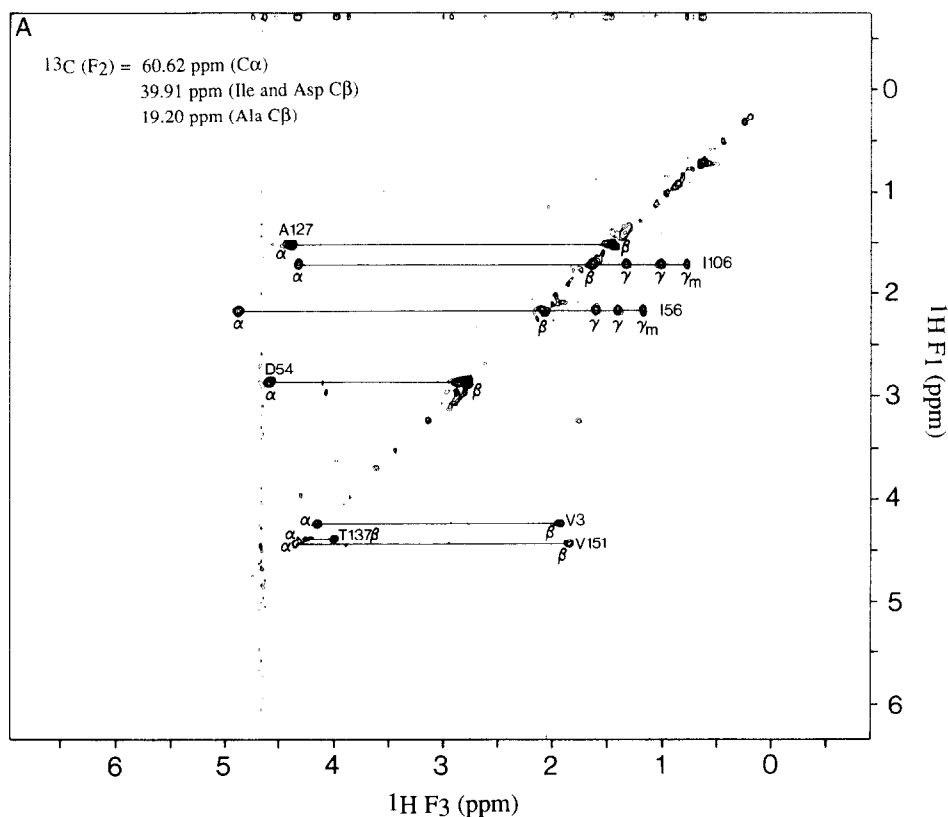


FIG. 2.  $F_1$ ,  $F_3$  slices of the 3D HCCH spectrum of interleukin-1 $\beta$ , recorded at 600 MHz. Because of extensive folding utilized in the  $F_2$  dimension, each slice corresponds to three  $^{13}\text{C}$  chemical shifts, indicated in each panel. Separation between slices in the  $F_2$  dimension is 0.32 ppm (48 Hz). Diagonal resonances correspond to one-bond correlations between  $^{13}\text{C}$  ( $F_2$ ) and  $^1\text{H}$  ( $F_1 = F_3$ ) chemical shifts; cross peaks originate from magnetization transfer to protons that are geminal or vicinal with respect to the protons on the diagonal.

caying envelope shape, resulting in a broader  $F_2$  linewidth than is observed for the cross peaks.

Figure 2 shows two ( $F_1$ ,  $F_3$ ) slices of the 3D spectrum of interleukin-1 $\beta$ . Assignment of the side-chain resonances in such slices is relatively straightforward once full sequence-specific assignments of the  $\text{C}\alpha$  carbons and  $\text{H}\alpha$  protons are available. Note that the  $\text{C}\alpha$  assignments for a protein the size of interleukin-1 $\beta$  usually cannot be obtained from a simple 2D  $^1\text{H}$ - $^{13}\text{C}$  correlation spectrum alone, because of the substantial degree of overlap in the  $\text{H}\alpha$  region of the spectrum. In the present case,  $\text{C}\alpha$  resonance assignments relied heavily on the use of a triple-resonance 3D experiment that correlates the backbone NH proton and  $^{15}\text{N}$  chemical shifts with those of the intrasidue  $\text{C}\alpha$  carbon (16). Complete assignments of the backbone proton and  $^{15}\text{N}$  resonances were obtained previously by using 3D NOESY-HMQC and NOESY-HOHAHA experiments (17).

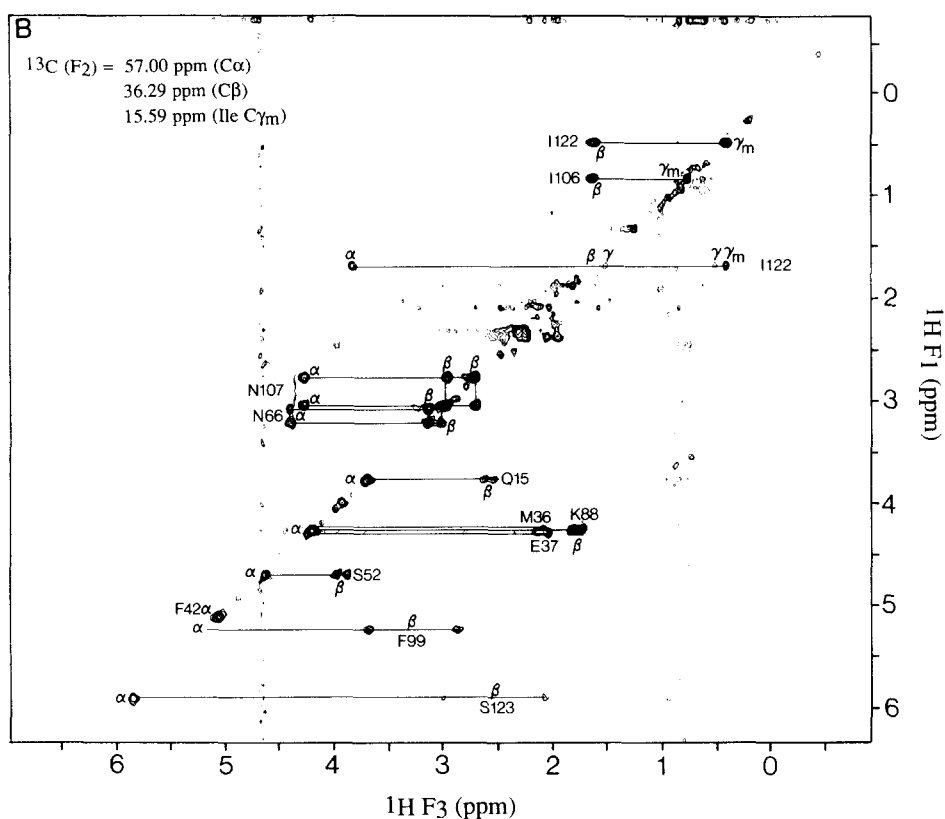


FIG. 2—Continued

The  $F_2$  spectral width was set to only 20.7 ppm, resulting in extensive folding in the  $^{13}\text{C}$  dimension. This folding affords a substantial increase in the  $F_2$  resolution, without introducing any serious ambiguities. Even though each of the slices shown in Fig. 2 has three possible  $^{13}\text{C}$  shift values associated with it, in all but very rare cases the  $F_3$  coordinates of the diagonal and cross peaks allow identification of the  $^{13}\text{C}$  shift value that corresponds to the diagonal peak. For example, in Fig. 2A, the most upfield labeled diagonal resonance (at 1.52 ppm) shows a single cross peak to a proton in the  $\text{C}\alpha$  region at 4.40 ppm, suggesting an alanine residue (Ala-127), and indicating that the appropriate diagonal peak has an  $F_2$  coordinate of 19.2 (and not 39.9) ppm. The adjacent diagonal resonance (originating from Ile-106) also shows a cross peak with an  $\text{H}\alpha$  resonance, but in addition, three more cross peaks to the two nonequivalent  $\text{C}\gamma$  methylene protons and to the  $\text{C}\gamma_m$  methyl protons are observed. This pattern of resonances is characteristic of an isoleucine residue, suggesting that the 39.9 (and not 19.2) ppm  $F_2$  shift corresponds to the diagonal resonance. In the few cases where it may not be immediately obvious which of the three possible  $F_2$  values applies, the slices in question are compared with those of the 3D NOESY-HMQC spectrum, which has been recorded with exactly twice the  $^{13}\text{C}$  spectral width (and only eight scans per  $t_1, t_2$ ), and for which no ambiguity is present.

The slices shown in Fig. 2 are asymmetric about the  $F_1 = F_3$  diagonal, because both diagonal and cross peaks are labeled with the  $^{13}\text{C}$  shift of the diagonal resonances. Thus, pairs of mirror image cross peaks appear in different slices. For example, Fig. 2A shows the correlation between Ile-106  $\text{H}\beta$  (diagonal) and Ile-106  $\text{C}\gamma\text{H}_3$  (cross peak). A slice taken at the  $^{13}\text{C}$  shift of the Ile-106  $\text{C}\gamma$  methyl carbon (Fig. 2B) shows the correlation between Ile-106  $\text{C}\gamma\text{H}_3$  (diagonal) and  $\text{H}\beta$  (cross peak). Figure 2B also shows the characteristic symmetric patterns observed for diagonal resonances of nonequivalent methylene protons, as seen for Asn-107 and Asn-66.

There are several diagonal resonances present in the slices shown in Fig. 2 for which no cross peaks appear. This is caused by the broader  $F_2$  lineshape of the diagonal resonances relative to the cross peaks, as discussed above. For example, the diagonal resonance of Phe-42  $\text{H}\alpha$  is clearly visible in Fig. 2B, whereas the cross peaks are absent in this slice. The adjacent slice, taken at  $F_2 = 56.67$  ppm, shows intense cross peaks to the  $\text{H}\beta$  protons (data not shown).

The resonance intensity obtainable in a regular one-dimensional refocused INEPT  $^{13}\text{C}$  spectrum is approximately equal for methine, methylene, and methyl carbons. This means that for methylene and methyl sites only one-half and approximately one-third of the  $^1\text{H}$  magnetization can be transferred into net  $^{13}\text{C}$  magnetization. Although a reverse INEPT transfers all  $^{13}\text{C}$  magnetization back to the protons, for two nonequivalent methylene protons, each receives only one-half of the  $^{13}\text{C}$  magnetization. The HCCH 3D technique employs a refocused INEPT transfer for magnetization transfer from protons to  $^{13}\text{C}$  and a reverse refocused INEPT transfer from  $^{13}\text{C}$  to protons. Therefore, correlations involving nonequivalent methylene protons are attenuated relative to magnetization transfer between vicinal methine protons. Thus, cross peaks between a methine and two nonequivalent methylene protons are attenuated twofold, and cross peaks between two pairs of nonequivalent methylene protons are attenuated fourfold. Correlations with methyl protons do not benefit from a threefold higher intensity, as observed in regular inverse detection experiments (18), but show the same intensity as cross peaks with methine protons. It is also easily calculated and confirmed experimentally that transfer via carbons with multiple  $^{13}\text{C}$  neighbors (for example, Ile- $\text{C}\beta$ ) is attenuated relative to transfer via carbons that have only a single  $^{13}\text{C}$  coupling partner (Ser, Asn, Asp, and Ala  $\text{C}\alpha$ - $\text{C}\beta$ ). Nevertheless, the spectra of Fig. 2 clearly indicate that the sensitivity obtainable in a 3 day experiment is sufficient to observe correlations between all types of vicinal protons.

The HCCH 3D spectrum provides nearly complete assignments of all aliphatic proton and  $^{13}\text{C}$  resonances, with the exception of some resonances of the long aliphatic side chains (e.g., Lys, Arg) for which substantial overlap remains, even in the 3D spectrum. With virtually complete assignments of both  $^1\text{H}$  and  $^{13}\text{C}$  resonances in hand, it becomes quite straightforward to make a detailed analysis of a 3D NOESY-HMQC (4, 5) spectrum, providing the necessary information for protein structure determination.

#### ACKNOWLEDGMENTS

We thank Dr. Paul Wingfield for the sample of uniformly  $^{15}\text{N}$ - and  $^{13}\text{C}$ -labeled interleukin- $1\beta$ . This work was supported by the Intramural AIDS Antiviral Program of the Office of the Director of the National

Institutes of Health (A.B., G.M.C., and A.M.G.). L.E.K. acknowledges financial support from the Medical Research Council of Canada and the Alberta Heritage Trust Foundation.

## REFERENCES

1. D. MARION, L. E. KAY, S. W. SPARKS, AND D. A. TORCHIA, *J. Am. Chem. Soc.* **111**, 1515 (1989).
2. E. R. P. ZUIDERWEG AND S. W. FESIK, *Biochemistry* **28**, 2387 (1989).
3. D. MARION, P. C. DRISCOLL, L. E. KAY, P. T. WINGFIELD, A. BAX, A. M. GRONENBORN, AND G. M. CLORE, *Biochemistry* **28**, 6150 (1989).
4. M. IKURA, L. E. KAY, R. TSCHUDIN, AND A. BAX, *J. Magn. Reson.* **86**, 204 (1990).
5. E. R. P. ZUIDERWEG, L. P. MCINTOSH, F. W. DAHLQUIST, AND S. W. FESIK, *J. Magn. Reson.* **86**, 210 (1990).
6. S. W. FESIK, R. T. GAMPE, AND E. R. P. ZUIDERWEG, *J. Am. Chem. Soc.* **111**, 770 (1989).
7. S. S. WIJENGA, K. HALLENGA, AND C. W. HILBERS, *J. Magn. Reson.* **84**, 634 (1989).
8. L. E. KAY, M. IKURA, AND A. BAX, *J. Am. Chem. Soc.* **112**, 888 (1990).
9. G. A. MORRIS AND R. FREEMAN, *J. Am. Chem. Soc.* **101**, 760 (1979).
10. D. P. BURUM AND R. R. ERNST, *J. Magn. Reson.* **39**, 163 (1980).
11. A. J. SHAKA, J. KEELER, AND R. FREEMAN, *J. Magn. Reson.* **53**, 313 (1983).
12. G. A. MORRIS AND R. FREEMAN, *J. Magn. Reson.* **29**, 433 (1978).
13. L. E. KAY, D. MARION, AND A. BAX, *J. Magn. Reson.* **84**, 72 (1989).
14. G. BODENHAUSEN, H. KOGLER, AND R. R. ERNST, *J. Magn. Reson.* **58**, 370 (1984).
15. M. H. LEVITT AND R. FREEMAN, *J. Magn. Reson.* **33**, 473 (1979).
16. M. IKURA, L. E. KAY, AND A. BAX, *Biochemistry*, submitted.
17. P. C. DRISCOLL, G. M. CLORE, D. MARION, P. WINGFIELD, AND A. M. GRONENBORN, *Biochemistry*, in press.
18. M. F. SUMMERS, L. G. MARZILLI, AND A. BAX, *J. Am. Chem. Soc.* **108**, 4285 (1986).
19. D. MARION, M. IKURA, R. TSCHUDIN, AND A. BAX, *J. Magn. Reson.* **85**, 393 (1989).